

Cite this: *J. Mater. Chem. C*, 2025, 13, 13190Achieving clear ferroelectric polarization reversal in room-temperature multiferroic  $\epsilon$ -Fe<sub>2</sub>O<sub>3</sub> systems through grain boundary engineering†Tsukasa Katayama,<sup>id</sup>\*<sup>ab</sup> Shintaro Yasui,<sup>\*c</sup> Takahisa Shiraishi,<sup>de</sup> Takanori Kiguchi,<sup>de</sup> Badari Narayana Rao,<sup>id</sup><sup>f</sup> Yosuke Hamasaki<sup>id</sup><sup>g</sup> and Mitsuru Itoh<sup>\*fh</sup>

$\epsilon$ -Fe<sub>2</sub>O<sub>3</sub>-related oxides are promising room-temperature multiferroic materials owing to their significant magnetization and switchable ferroelectric polarization. However, their large leakage current hinders the quality of ferroelectric polarization reversal, limiting research despite superior magnetic properties compared to the well-studied BiFeO<sub>3</sub> system. This study addresses these limitations through two investigations. First, we investigate the difficulty of polarization reversal by analyzing grain boundary structures in  $\epsilon$ -Fe<sub>2</sub>O<sub>3</sub>-related epitaxial films, which inherently form due to their non-perovskite orthorhombic structure. Second, we enhance polarization reversal *via* grain boundary engineering. Our findings reveal that these films contain numerous small grains (250–770 nm<sup>2</sup>) with Fe<sup>2+/3+</sup> states at grain boundaries, where approximately 40% act as ferroelectric domain walls. The high grain boundary density causes significant leakage current and hinders polarization reversal. By implementing a codoping method, we successfully reduce the grain boundary density, achieving clear ferroelectric hysteresis. This breakthrough highlights the potential of  $\epsilon$ -Fe<sub>2</sub>O<sub>3</sub>-related oxides as room-temperature multiferroic materials with substantial magnetization and offers new prospects for research on materials distinct from the BiFeO<sub>3</sub> system.

Received 18th February 2025,  
Accepted 15th May 2025

DOI: 10.1039/d5tc00689a

rsc.li/materials-c

## 1. Introduction

Multiferroic materials are a fascinating class of materials that exhibit both ferroelectric and ferromagnetic properties within a single phase. This dual nature has the potential to advance fundamental physics and enable innovative applications, such as rapid data writing, energy-efficient devices, and secure data

storage, and hence, multiferroic materials have attracted considerable interest.<sup>1,2</sup> However, the coexistence of ferroelectric and magnetic behavior at room temperature remains rare. Two categories of room-temperature multiferroic materials have been identified: oxide materials related to BiFeO<sub>3</sub><sup>3–9</sup> and  $\epsilon$ -Fe<sub>2</sub>O<sub>3</sub>.<sup>10–25</sup> Materials in these two categories differ substantially in their crystal structures as well as their intrinsic properties.

The BiFeO<sub>3</sub>-related oxides with a perovskite structure are distinguished by their ability to achieve clear ferroelectric polarization (*P*) reversal under an applied electric field (*E*). These materials exhibit excellent piezoelectric properties, with a remanent polarization (*P<sub>r</sub>*) of approximately 60  $\mu\text{C cm}^{-2}$  and a piezoelectric coefficient (*d*<sub>33</sub>) of 70 pm V<sup>-1</sup>.<sup>3,4</sup> The coupling between the magnetic moment direction and polarization direction in BiFeO<sub>3</sub> allows for the modification of the magnetic moment orientation *via* *E*-induced polarization reversal at room temperature.<sup>5–7</sup> However, as BiFeO<sub>3</sub> exhibits antiferromagnetic ordering, the remanent magnetization (*M<sub>r</sub>*) is nearly zero.<sup>8</sup> Although the spin structure can be tuned by substrate-induced strain or chemical substitution (*e.g.*, Co doping), the *M<sub>r</sub>* value is still limited.<sup>9</sup>

In contrast,  $\epsilon$ -Fe<sub>2</sub>O<sub>3</sub>-related oxides exhibit substantial magnetization and coercive force at room temperature due to their ferrimagnetic nature.<sup>10–14</sup> For instance, Rh doping leads to a

<sup>a</sup> Research Institute for Electronic Science, Hokkaido University, N20W10, Kita, Sapporo 001-0020, Japan<sup>b</sup> JST-PRESTO, Kawaguchi, Saitama 332-0012, Japan.

E-mail: katayama@es.hokudai.ac.jp

<sup>c</sup> Laboratory for Zero-Carbon Energy, Institute of Science Tokyo, 2-12-1, Ookayama, Meguro-ku, Tokyo 152-8550, Japan. E-mail: yasui.s.aa@m.titech.ac.jp<sup>d</sup> Department of Materials Science, Graduate School of Science and Technology, Kumamoto University, 2-39-1 Kurokami, Chuo-ku, Kumamoto 860-8555, Japan<sup>e</sup> Magnesium Research Center, Kumamoto University, 2-39-1 Kurokami, Chuo-ku, Kumamoto 860-8555, Japan<sup>f</sup> Laboratory for Materials and Structures, Institute of Science Tokyo, 4259,

Nagatsuta-cho, Midori-ku, Yokohama 226-8501, Japan.

E-mail: mitsuru\_itoh@icloud.com

<sup>g</sup> Department of Applied Physics, National Defense Academy, Yokosuka 239-8686, Japan<sup>h</sup> Environmental Safety Center, Institute of Science Tokyo, 4259 Nagatsuta-cho, Midori-ku, Yokohama 226-8501, Japan† Electronic supplementary information (ESI) available: TEM images and STEM-EELS data. See DOI: <https://doi.org/10.1039/d5tc00689a>

remarkable coercive force of 24 kOe, the highest value among oxide magnets, and Ga doping increases  $M_r$  to  $0.6\mu_B$  f.u.<sup>-1</sup> at 300 K.<sup>10</sup> These oxides have been investigated for applications related to their magnetic properties, including photo-induced magnetization reversal memory<sup>11</sup> and millimeter-wave absorption.<sup>12,13</sup> Moreover,  $E$ -induced polarization reversal has been demonstrated in thin-film  $\epsilon$ -Fe<sub>2</sub>O<sub>3</sub>-related oxides at room temperature.<sup>15–25</sup> However, the reported  $P$ - $E$  hysteresis loops indicate significant leakage currents, which hinder the quality of ferroelectric polarization reversal.  $\epsilon$ -Fe<sub>2</sub>O<sub>3</sub>-related oxides have not been extensively investigated in the field of multiferroics because they exhibit relatively poor polarization reversal properties in comparison to BiFeO<sub>3</sub>. Nonetheless, given the excellent magnetic properties of  $\epsilon$ -Fe<sub>2</sub>O<sub>3</sub>-related oxides, establishing clear design guidelines for achieving reliable electric-field-induced ferroelectric polarization reversal can help significantly improve their multiferroic application prospects.

The reason for the difficulty in achieving ferroelectric polarization reversal in  $\epsilon$ -Fe<sub>2</sub>O<sub>3</sub>-related oxides remains unclear. The challenge is attributed primarily to their unique crystal structure, which deviates from the common perovskite structure of BiFeO<sub>3</sub>. The crystal structure of  $\epsilon$ -Fe<sub>2</sub>O<sub>3</sub> comprises octahedral (O<sub>h</sub>) Fe<sub>A</sub>, Fe<sub>B</sub>, and Fe<sub>C</sub> sites, as well as tetrahedral (T<sub>d</sub>) Fe<sub>D</sub> sites (Fig. 1(a)). The presence of grain boundaries (GBs) in the films further complicates the issue: thin films reported in the literature consist of three types of in-plane grains with the polar axis ( $c$ -axis) oriented along the out-of-plane direction (Fig. 1(b)).

This study has two key objectives. First, we aim to elucidate the grain boundary structure and identify the factors hindering polarization reversal. Second, we explore grain boundary engineering as a strategy to achieve clear ferroelectric polarization reversal. We investigate the grain structures *via* plan-view and cross-sectional transmission electron microscopy (TEM) and high-angle annular dark-field scanning TEM (HAADF-STEM) measurements on three types of  $\epsilon$ -Fe<sub>2</sub>O<sub>3</sub>-related oxide films: Ga<sub>0.8</sub>Fe<sub>1.2</sub>O<sub>3</sub>, Sc<sub>0.5</sub>Fe<sub>1.5</sub>O<sub>3</sub>, and Ga<sub>0.4</sub>Sc<sub>0.2</sub>Fe<sub>1.4</sub>O<sub>3</sub>. Hereafter,

these films are referred to as Ga-doped, Sc-doped, and (Ga,Sc)-codoped  $\epsilon$ -Fe<sub>2</sub>O<sub>3</sub> films, respectively.

Our findings revealed that the films contained significantly small grains, with the average sizes ranging from 250 to 770 nm<sup>2</sup>. Fe<sup>2+/3+</sup> states were present at the GBs, and approximately 40% of the GBs corresponded to ferroelectric domain walls. This high density of GBs was identified as the primary source of the large leakage current and the reason for the difficulty in achieving polarization reversal. Furthermore, Ga and Sc codoping reduced the density of GBs, enabling clear ferroelectric polarization reversal in the films.

## 2. Results and discussion

### 2.1. Domain wall structure characteristics

Fig. 1(c) illustrates the  $2\theta$ - $\theta$  X-ray diffraction (XRD) patterns of the Ga-doped  $\epsilon$ -Fe<sub>2</sub>O<sub>3</sub> film. The 002, 004, and 006 XRD peaks were clearly observed, indicating that a  $c$ -axis-oriented film with an  $\epsilon$ -Fe<sub>2</sub>O<sub>3</sub> structure was obtained. As illustrated in the  $\phi$ -scan results (Fig. 1(d)), the film exhibited sixfold in-plane symmetry, whereas the STO(111) plane exhibited threefold symmetry. Considering the orthorhombic structure of  $\epsilon$ -Fe<sub>2</sub>O<sub>3</sub>, the film consisted of three types of in-plane grains,  $G_1$ ,  $G_2$ , and  $G_3$ , which were rotated by 120° relative to each other as illustrated in Fig. 1(b).

Fig. 2(a) illustrates a plan-view TEM image of the Ga-doped  $\epsilon$ -Fe<sub>2</sub>O<sub>3</sub> film. Stripe-like patterns were observed. Compared with the Fe<sub>B</sub> and Fe<sub>C</sub> sites (blue and light blue circles in Fig. 1(a)), the Fe<sub>A</sub> and Fe<sub>D</sub> sites (orange and green points) are expected to be more clearly observed in the plan-view TEM image because they overlap along the out-of-plane direction. Thus, the stripe-like patterns were derived from the zigzag lines of the Fe<sub>A</sub> and Fe<sub>D</sub> atoms, which correspond to the orange and green lines in Fig. 1. The direction of the grains in the plan-view TEM image was determined based on the direction of the stripe-like

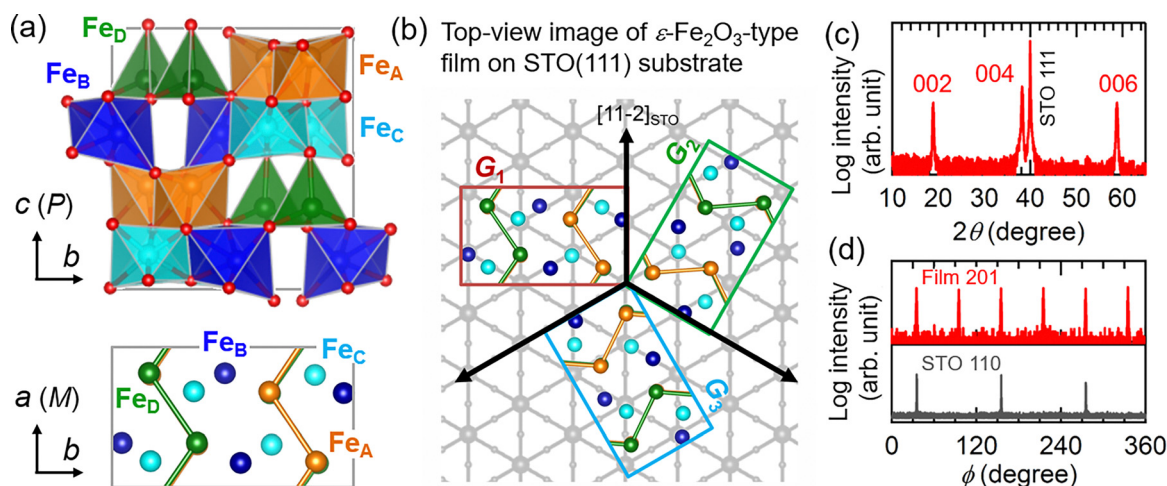


Fig. 1 (a) Crystal structures of  $\epsilon$ -Fe<sub>2</sub>O<sub>3</sub> and (b) top-view schematic of the  $\epsilon$ -Fe<sub>2</sub>O<sub>3</sub>-related oxide film grown on the STO(111) substrate. (c)  $2\theta$ - $\theta$  X-ray diffraction pattern and (d)  $\phi$ -scan of the Ga-doped  $\epsilon$ -Fe<sub>2</sub>O<sub>3</sub> film.



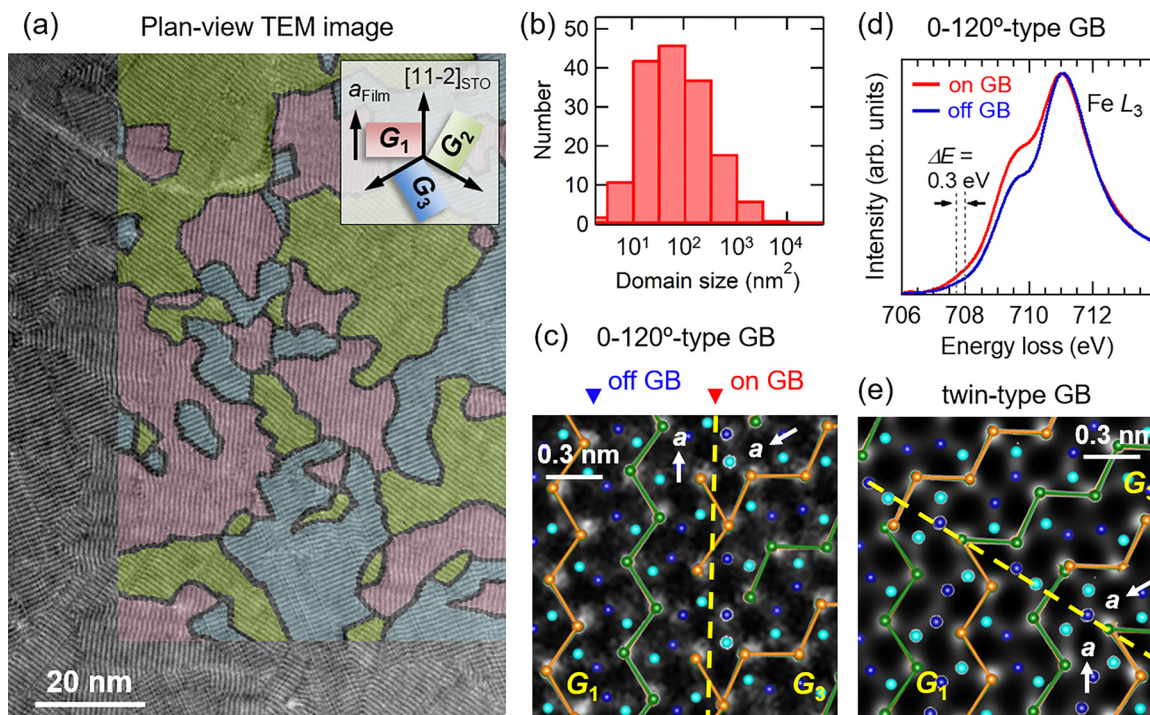


Fig. 2 (a) Plan-view TEM image. (b) A histogram of the grain size. (c) Plan-view STEM image and (d) on- and off-GB Fe  $L_3$ -edge EELS spectra near the 0–120°-type grain boundaries (GBs). (e) Plan-view STEM image near twin-type GBs for the Ga-doped  $\epsilon$ -Fe $_2$ O $_3$  film.

patterns. The  $G_1$ ,  $G_2$ , and  $G_3$  grain types are colored red, green, and blue, respectively, in Fig. 2(a). Fig. 2(b) illustrates a histogram of the grain size. The average size was as small as 250 nm $^2$ . These small grains formed a nanomosaic-like pattern in the film.

The GB structure was investigated *via* HAADF-STEM measurements. Typical GB structures were 0–120°-type and twin-type, as illustrated in Fig. 2(c) and (e), respectively. The 0–120°-type GB was formed by the connection between a (100) grain and a (110) grain. This connection is preferred because the  $a$ -axis length (5.06 Å) matches well with the value of  $b/\sqrt{3}$  (5.06 Å). In the twin-type GB, the mirror plane was formed in the direction parallel to the (110) plane, which crossed all cation sites. Although  $\epsilon$ -Fe $_2$ O $_3$  exhibits spontaneous polarization along the  $c$ -axis, and thus no intrinsic in-plane polarization is expected, the formation of twin-type grain boundaries could induce strain that may locally generate in-plane polarization components. Further investigation is required to clarify this possibility.

Fig. 2(d) and Fig. S1 (ESI $^\dagger$ ) illustrate the Fe  $L$ -edge electron energy loss spectroscopy (EELS) plots for the 0–120°-type GB (on-GB) and within the grain (off-GB). Both spectra exhibited prominent and left-shoulder peaks at 711 and 709.5 eV, respectively. The intensity of the shoulder peak in the on-GB spectrum was higher than that in the off-GB spectrum, indicating the reduced valence state of the Fe ions in the GB. The difference in the starting energy of the peak ( $\Delta E$ ) between the on- and off-GB regions was 0.3 eV. Thus, the valence state of the Fe ions in the GB is expected to be  $\sim 2.8^+$ . $^{26}$  This implies that oxygen vacancies were generated in the GB.

The GB structure was also investigated *via* cross-sectional HAADF-STEM measurements. In the HAADF-STEM measurements, the electron beam was irradiated in the  $[11-2]_{\text{STO}}$  direction (Fig. 3(a)). Fig. 3(b) shows the cross-sectional images of  $\epsilon$ -Fe $_2$ O $_3$  in the  $G_1$  and  $G_3$  domains. The atomic arrangement, marked in yellow boxes, can be used to determine the polarization direction. For example, when  $\epsilon$ -Fe $_2$ O $_3$  exhibits an upward polarization (up- $P$ ) in the  $G_1$  domain, the positions of the four atoms in the yellow box change to down-up-up-down. Meanwhile, in the up- $P$   $G_3$  domain, the three atoms in the yellow box have an up-down-up arrangement.

Fig. 3(c) illustrates a cross-sectional HAADF-STEM image of the region near the GB. Based on the atomic arrangement, the left and right domains were identified as up- $P$   $G_1$  and up- $P$   $G_3$ , respectively. We also observed GBs between the domains with opposite  $P$  directions (Fig. 3(d)). We observed 12 GBs in the Ga-doped  $\epsilon$ -Fe $_2$ O $_3$  film and found that five of them were formed between grains with opposite  $P$  directions. This suggests that approximately 40% of the GBs are ferroelectric 180°-domain walls (FE DWs).  $\epsilon$ -Fe $_2$ O $_3$  has four layers along the  $c$ -axis (Fig. 4(a)): L1 and L3 layers consisting of Fe $_A$  and Fe $_D$  sites and L2 and L4 layers consisting of Fe $_B$  and Fe $_C$  sites. The L1 layer of one grain was connected to either the L1 or L3 layer of another grain in all the observed GBs.

## 2.2. The origin of the difficulty in obtaining clear ferroelectric reversal

We identified the 0–120°-type GB structure from the plan-view and cross-sectional STEM measurements. Fig. 4(b) illustrates the 0–120°-type GBs between the up- $P$   $G_1$  and up- $P$   $G_3$  grains.



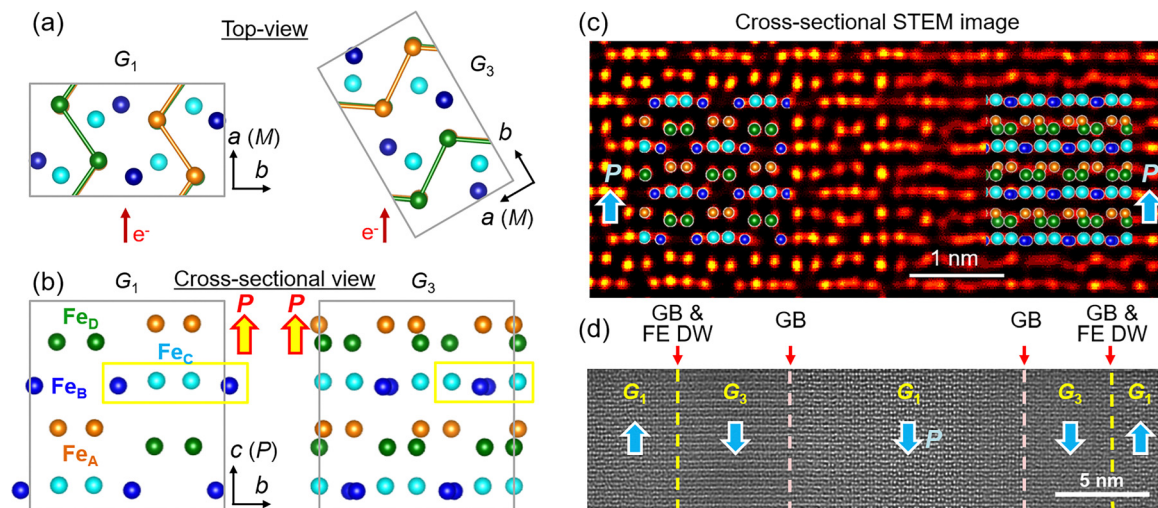


Fig. 3 (a) Top-view and (b) cross-sectional images of  $\epsilon$ - $\text{Fe}_2\text{O}_3$ . (c) and (d) Cross-sectional HAADF-STEM images of the Ga-doped  $\epsilon$ - $\text{Fe}_2\text{O}_3$  film.

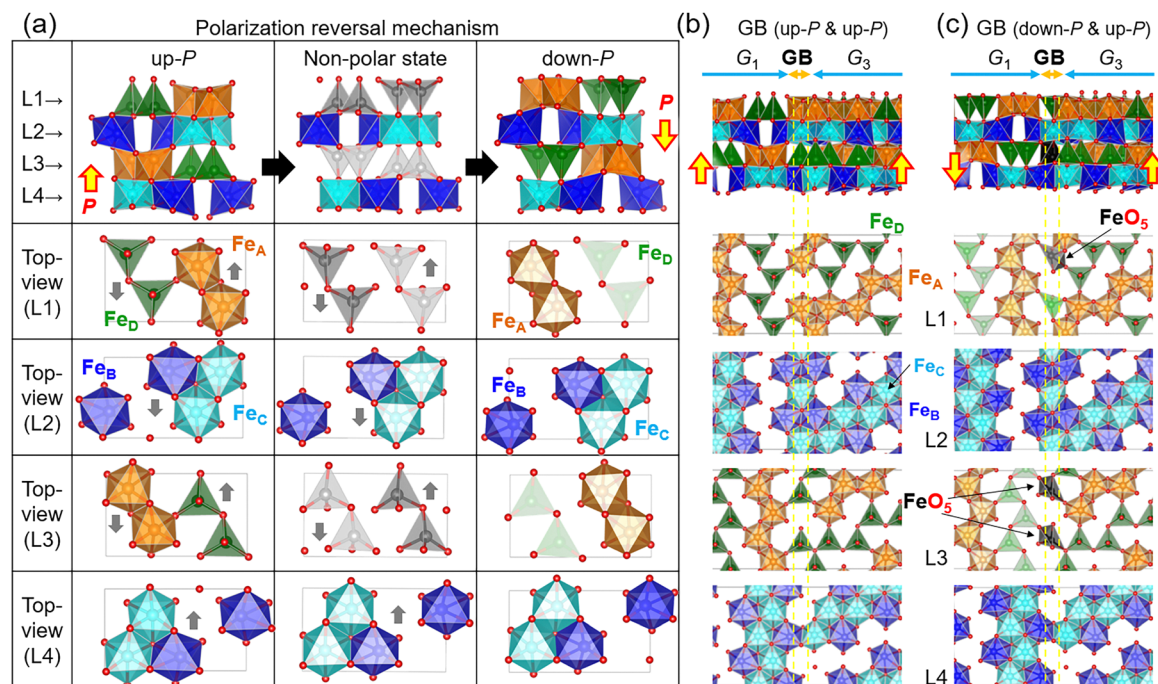


Fig. 4 (a)  $P$ -reversal mechanism in  $\epsilon$ - $\text{Fe}_2\text{O}_3$ . (b)  $0-120^\circ$ -type GB structure between the up- $P$   $G_1$  and up- $P$   $G_3$  domains. (c) Expected GB structure after  $P$  reversal in the  $G_1$  domain.

New cationic arrangements, such as  $\text{Fe}_D$ -site tetrahedron trimers, were observed in the GB.  $\epsilon$ - $\text{Fe}_2\text{O}_3$  is known to have a unique  $P$ -reversal mechanism.<sup>16,17</sup> During  $P$  reversal, the octahedral ( $\text{O}_h$ )  $\text{Fe}_A$  and tetrahedral ( $\text{T}_d$ )  $\text{Fe}_D$  sites in the L1 and L3 layers were switched, while  $\text{Fe}_B$  and  $\text{Fe}_C$  sites in the L2 and L4 layers were shifted along the  $a$ -axis (Fig. 4(a)). Fig. 4(c) illustrates the expected GB structure after  $P$  reversal in the  $G_1$  domain. Pyramidal  $\text{FeO}_5$  appeared in the GB in the L1 and L3 layers after  $P$  reversal. In addition, the connection between the  $\text{Fe}_B$  and  $\text{Fe}_C$  sites was slightly distorted in the L2 and L4 layers. Thus, the activation energy for  $P$  reversal increased near the GB; in other words,  $P$  reversal was restricted by the GBs in the film. X. Guan *et al.* conducted *in situ*

STEM observations while applying an electric field to  $\epsilon$ - $\text{Fe}_2\text{O}_3$  films and reported that ferroelectric switching tends to occur more readily near ferroelectric domain walls within a single grain.<sup>27</sup> This finding supports the idea that reducing the density of grain boundaries—which inhibit ferroelectric switching—and increasing grain size are crucial for improving ferroelectric properties.

### 2.3. Achieving clear ferroelectric reversal *via* domain engineering

Obtaining a good ferroelectric hysteresis loop in  $\epsilon$ - $\text{Fe}_2\text{O}_3$ -related oxides is challenging. We found that this difficulty is due to the high density of GBs with  $\text{Fe}^{2+/3+}$  states, which inhibits  $P$



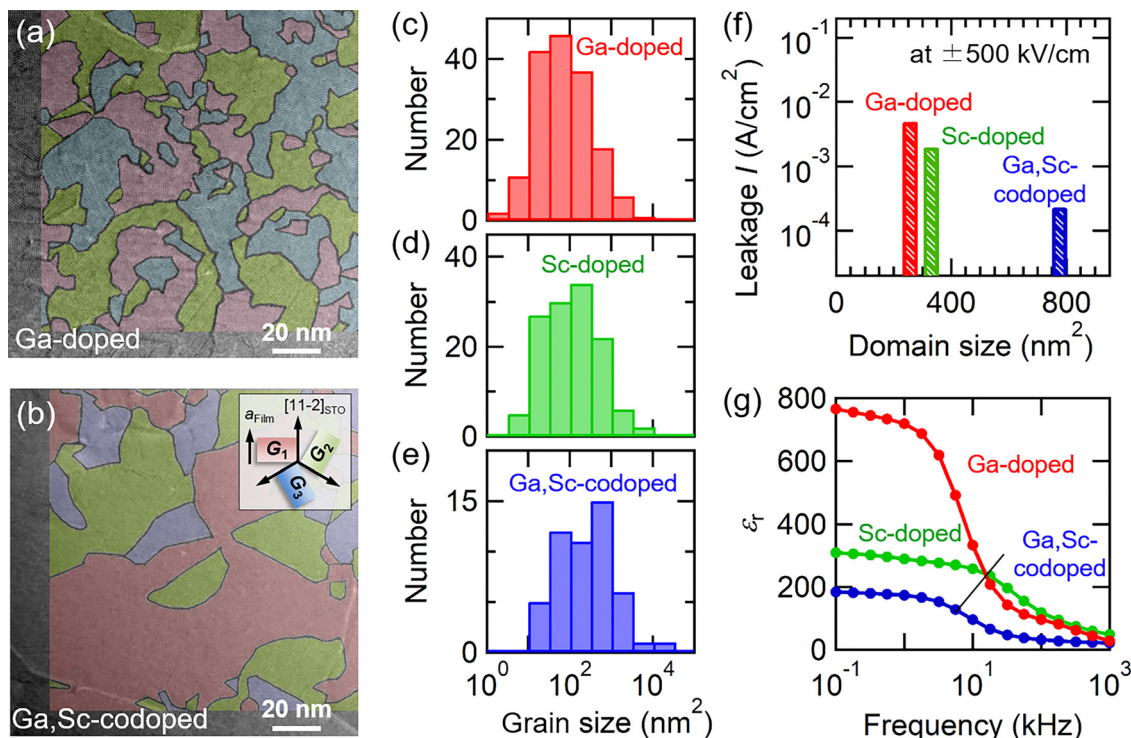


Fig. 5 Plan-view TEM images and histograms of the grain size for the (a) and (c) Ga-doped, (d) Sc-doped, and (b) and (e) Ga,Sc-codoped  $\epsilon$ - $\text{Fe}_2\text{O}_3$  films. (f) Leakage current and (g) permittivity of the films at 300 K.

reversal, as shown in Fig. 4. Therefore, we attempted to increase the grain size through chemical substitution. Fig. 5(a)–(e) and Fig. S2 (ESI<sup>†</sup>) illustrate the plan-view TEM images and histograms of the grain size for the Ga-doped, Sc-doped, and Ga,Sc-codoped  $\epsilon$ - $\text{Fe}_2\text{O}_3$  films. The average grain size of the Ga,Sc-codoped film ( $770 \text{ nm}^2$ , Fig. 5(e)) was three times larger than that of the Ga-doped film ( $250 \text{ nm}^2$ , Fig. 5(c)). This may be attributed to two reasons. First, new cationic arrangements, such as  $\text{Fe}_\text{D}$ -site tetrahedron trimers, are formed at the GBs. However, such cationic arrangements may be unstable depending on the elemental species, which, in turn, may increase the energy required for GB formation. Second, the difference between the  $a$ -axis length and  $b/\sqrt{3}$  value leads to strain near the GBs and results in an increase in the energy required for GB formation. Further investigation is necessary to elucidate the reasons in detail.

Fig. 5(f) illustrates the leakage current ( $I$ ) for the films at  $\pm 500 \text{ kV cm}^{-1}$ . The  $I$  value decreases with increasing grain size, reflecting the reduction in the number of the GBs with  $\text{Fe}^{2+/3+}$  state. Fig. 5(g) illustrates the frequency dependence of the dielectric constants ( $\epsilon'$ ) of the films. The films exhibit relaxation frequencies of 10–50 kHz due to dielectric relaxation through oxygen vacancies, which are coupled with the  $\text{Fe}^{2+}$  ions.<sup>21</sup>  $\epsilon'$  tends to decrease, particularly below the relaxation frequency, with an increase in the grain size because of the reduction in the number of oxygen vacancies that are located at the GBs.

Fig. 6(a) illustrates the  $P$  versus electric field ( $P$ – $E$ ) hysteresis loops for the Sc-doped and Ga,Sc-codoped  $\epsilon$ - $\text{Fe}_2\text{O}_3$  films at 300 K. The Ga-doped film did not exhibit ferroelectric behavior

in the  $P$ – $E$  curve because of the high density of GBs, as discussed in Section 2.2. In contrast, the Sc- and Ga,Sc-codoped films exhibited clear ferroelectric hysteresis loops with minimal leakage currents in the  $P$ – $E$  curves. The remanent polarizations ( $P_r$ ) of the Sc-doped and Ga,Sc-codoped films were  $3.5$  and  $4.5 \mu\text{C cm}^{-2}$ , respectively. The obtained  $P_r$  values were smaller than the calculated values for  $\text{GaFeO}_3$ -type  $\text{Fe}_2\text{O}_3$  ( $21 \mu\text{C cm}^{-2}$ ) and  $\text{GaFeO}_3$  ( $25 \mu\text{C cm}^{-2}$ ).<sup>16,17,28</sup> The decrease in  $P_r$  with decreasing grain size is also observed in ferroelectric  $\text{Pb}(\text{Zr}_x\text{Ti}_{1-x})\text{O}_3$ .<sup>29</sup> This is attributed primarily to the pinning of ferroelectric domains at the GBs due to the high activation energy of polarization reversal at the GBs. Thus, a strong relationship between the ferroelectric properties and GBs exists in  $\epsilon$ - $\text{Fe}_2\text{O}_3$ -related oxide films, and increasing the grain size is key to improving their ferroelectric properties. The Sc-doped and Ga,Sc-codoped films also exhibited ferrimagnetic properties at 300 K (Fig. 6(b)), confirming the coexistence of spontaneous polarization and magnetization at room temperature.

### 3. Conclusion

The GB structures of room-temperature multiferroic  $\epsilon$ - $\text{Fe}_2\text{O}_3$ -related oxide films were investigated *via* plan-view and cross-sectional TEM and STEM measurements. The grain sizes of the films were as small as  $250$ – $770 \text{ nm}^2$ . The STEM-EELS measurements revealed that the valence state of Fe was reduced at the GBs. Cross-sectional STEM measurements indicated that approximately 40% of the GBs were FE DWs. The large leakage current and the difficulty in achieving good  $P$  reversal behavior



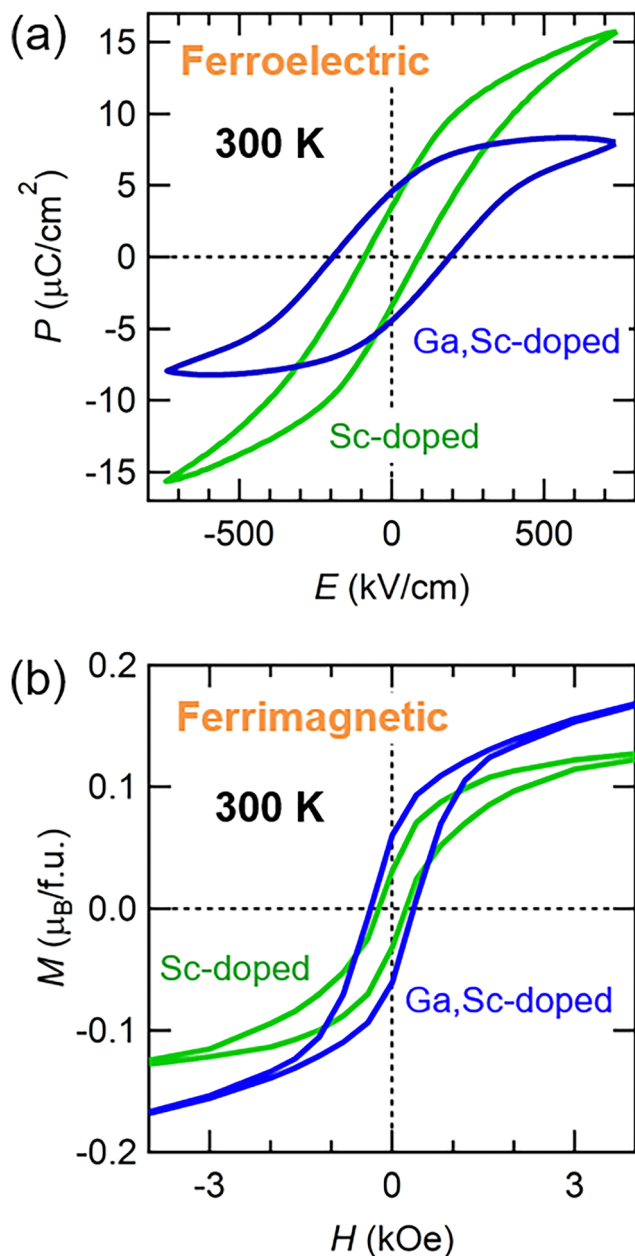


Fig. 6 (a) Polarization ( $P$ ) versus electric field ( $E$ ) and (b) magnetization ( $M$ ) versus magnetic field ( $H$ ) curves for the Sc-doped and Ga,Sc-codoped  $\epsilon$ - $\text{Fe}_2\text{O}_3$  films at 300 K.

in  $\epsilon$ - $\text{Fe}_2\text{O}_3$ -related oxide films were attributed to the high density of GBs. Therefore, we reduced the density of GBs *via* codoping and achieved clear ferroelectric hysteresis with minimal leakage current. The results obtained in this study are expected to catalyze further research on room-temperature multiferroic materials with large magnetization distinct from the  $\text{BiFeO}_3$  system.

## 4. Experimental

The Ga-doped, Sc-doped, and Ga,Sc-codoped  $\epsilon$ - $\text{Fe}_2\text{O}_3$  films were fabricated on  $\text{SrTiO}_3(111)$  (STO) and Nb 0.5 wt%-doped

STO(111) substrates *via* pulsed laser deposition. The chemical compositions of the films were  $\text{Ga}_{0.8}\text{Fe}_{1.2}\text{O}_3$ ,  $\text{Sc}_{0.5}\text{Fe}_{1.5}\text{O}_3$ , and  $\text{Ga}_{0.4}\text{Sc}_{0.2}\text{FeO}_3$ , respectively. The substrate temperature and oxygen partial pressure during the deposition were maintained at 700 °C and 200 mTorr, respectively. The fourth harmonic of an Nd:YAG pulsed laser (wavelength: 266 nm) was used with an energy of 12 mJ per pulse and a repetition rate of 5 Hz. The laser spot size was approximately 1 mm<sup>2</sup>, and the distance between the target and the substrate was 50 mm. The typical thickness of the films was 30–40 nm.

The crystal structures of the films were determined *via* high-resolution XRD with  $\text{Cu-K}\alpha_1$  radiation (Rigaku Smartlab). The microstructure was investigated *via* TEM and HAADF-STEM measurements using a JEM-ARM200F cold FEG instrument. In our EELS measurements, the acquisition points were manually selected by observing the STEM image in real time, as our system does not include an automated protocol for positioning EELS measurements. We performed the EELS measurements several times, and during the process, we observed instances of apparent chemical shifts. However, we only used data sets that showed minimal chemical shift and in which the EELS acquisition point clearly coincided with the grain boundary location in the STEM image. The leakage current was measured *via* the conventional two-probe method (Keithley 2450 SourceMeter) at room temperature. We did not use the step relaxation method for the leakage current measurements. Instead, the current–voltage ( $I$ – $V$ ) characteristics were measured by applying a voltage in steps of 0.1 seconds per voltage point. The dielectric properties were measured using a precision LCR meter (Agilent, 4284A) at room temperature. The ferroelectric properties were investigated using a ferroelectric tester (Toyo Corporation FCE-1E) at room temperature. The ferroelectric hysteresis loops were performed at a frequency of 10 kHz. Pt electrodes and Nb:STO substrates were respectively used as the top and bottom electrodes while measuring the leakage current, dielectric properties, and ferroelectric properties. The diameter of the Pt electrodes used for the ferroelectric and leakage current measurements was 100  $\mu\text{m}$ , and that of the Pt electrodes used for the dielectric measurements was 200  $\mu\text{m}$ . The magnetization of the films was measured using a superconducting quantum interference device magnetometer (Quantum Design, MPMS XL).

## Data availability

All data supporting the findings of this study are included in the main manuscript.

## Conflicts of interest

There are no conflicts to declare.

## Acknowledgements

This study was partially supported by JST PRESTO (JPMJPR21Q3), JST A-STEP (JPMJTR24032140), JSPS KAKENHI Grants-in-Aid



(22H01768), and Tohoku univ. CINTS (A-18-TU-0013, A-17-TU-0009, A-16-TU-0038).

## References

- 1 T. Kimura, T. Goto, H. Shintani, K. Ishizaka, T. Arima and Y. Tokura, Magnetic control of ferroelectric polarization, *Nature*, 2003, **426**, 55.
- 2 J. F. Scott, Multiferroic memories, *Nat. Mater.*, 2007, **6**, 256.
- 3 J. Wang, *et al.*, Epitaxial BiFeO<sub>3</sub> Multiferroic Thin Film Heterostructures, *Science*, 2003, **299**, 5613.
- 4 D. Lebeugle, *et al.*, Room-temperature coexistence of large electric polarization and magnetic order in BiFeO<sub>3</sub> single crystals, *Phys. Rev. B: Condens. Matter Mater. Phys.*, 2007, **76**, 024116.
- 5 K. Shimizu, *et al.*, Direct Observation of Magnetization Reversal by Electric Field at Room Temperature in Co-Substituted Bismuth Ferrite Thin Film, *Nano Lett.*, 2019, **19**, 1767.
- 6 N. Waterfield Price, *et al.*, Electrical Switching of Magnetic Polarity in a Multiferroic BiFeO<sub>3</sub> Device at Room Temperature, *Phys. Rev. Appl.*, 2017, **8**, 014033.
- 7 P. Meisenheimer, *et al.*, Switching the spin cycloid in BiFeO<sub>3</sub> with an electric field, *Nat. Commun.*, 2024, **15**, 2903.
- 8 H. Béa, *et al.*, Influence of parasitic phases on the properties of BiFeO<sub>3</sub> epitaxial thin films, *Appl. Phys. Lett.*, 2005, **87**, 072508.
- 9 M. Azuma, H. Hojo, K. Oka, H. Yamamoto, K. Shimizu, K. Shigematsu and Y. Sakai, Functional Transition Metal Perovskite Oxides with 6s<sup>2</sup> Lone Pair Activity Stabilized by High-Pressure Synthesis., *Annu. Rev. Mater. Res.*, 2021, **51**, 329–349.
- 10 A. Namai, M. Yoshikiyo, K. Yamada, S. Sakurai, T. Goto, T. Yoshida, T. Miyazaki, M. Nakajima, T. Suemoto, H. Tokoro and S. Ohkoshi, Hard magnetic ferrite with a gigantic coercivity and high frequency millimetre wave rotation, *Nat. Commun.*, 2012, **3**, 1035.
- 11 S. Ohkoshi, K. Imoto, A. Namai, M. Yoshikiyo, S. Miyashita, H. Qiu, S. Kimoto, K. Kato and M. Nakajima, Rapid Faraday Rotation on  $\epsilon$ -Iron Oxide Magnetic Nanoparticles by Visible and Terahertz Pulsed Light, *J. Am. Chem. Soc.*, 2019, **141**(4), 1775–1780.
- 12 S. Ohkoshi, S. Kuroki, S. Sakurai, K. Matsumoto, K. Sato and S. Sasaki, A millimeter-wave absorber based on gallium-substituted  $\epsilon$ -iron oxide nanomagnets, *Angew. Chem., Int. Ed.*, 2007, **46**, 8392–8395.
- 13 S. Tsukamoto, Y. Oki, K. Imoto, A. Namai, M. Yoshikiyo and S. Ohkoshi, Resonance Frequency Tuning of a 200 GHz Band Absorber by an External Magnetic Field, *Adv. Photonics Res.*, 2022, **3**, 2100319.
- 14 J. Jin, S. Ohkoshi and K. Hashimoto, Giant coercive field of nanometer-sized iron oxide, *Adv. Mater.*, 2004, **16**, 48.
- 15 S. Mukherjee, A. Roy, S. Auluck, R. Prasad, R. Gupta and A. Garg, Room temperature nanoscale ferroelectricity in magnetoelectric GaFeO<sub>3</sub> epitaxial thin films, *Phys. Rev. Lett.*, 2013, **111**, 087601.
- 16 K. Xu, J. S. Feng, Z. P. Liu and H. J. Xiang, Origin of ferrimagnetism and ferroelectricity in room-temperature multiferroic  $\epsilon$ -Fe<sub>2</sub>O<sub>3</sub>, *Phys. Rev. Appl.*, 2018, **9**, 044011.
- 17 B. N. Rao, A. Yasui, T. Katayama, A. Taguchi, H. Moriwake, Y. Hamasaki and M. Itoh, Investigation of ferrimagnetism and ferroelectricity in Al<sub>x</sub>Fe<sub>2-x</sub>O<sub>3</sub> thin films, *J. Mater. Chem. C*, 2020, **8**, 706.
- 18 H. Wang, Y. Zhang, K. Tachiyama, Z. Xia, J. Fang, Q. Li, G. Cheng, Y. Shi, J. Yu, T. Katayama, S. Yasui and M. Itoh, Large Polarization Switching and High-Temperature Magnetolectric Coupling in Multiferroic GaFeO<sub>3</sub> Systems, *Inorg. Chem.*, 2021, **60**, 225.
- 19 M. Gich, I. Fina, A. Morelli, F. Sánchez, M. Alexe, J. Gàzquez, J. Fontcuberta and A. Roig, Multiferroic iron oxide thin films at room temperature, *Adv. Mater.*, 2014, **26**, 4645.
- 20 S. Song, H. M. Jang, N. Lee, J. Y. Son, R. Gupta, A. Garg, J. Ratanapreechachai and J. F. Scott, Ferroelectric polarization switching with a remarkably high activation energy in orthorhombic GaFeO<sub>3</sub> thin films, *NPG Asia Mater.*, 2016, **8**, e242.
- 21 T. Katayama, S. Yasui, Y. Hamasaki, T. Shiraishi, A. Akama, T. Kiguchi and M. Itoh, Ferroelectric and magnetic properties in room-temperature multiferroic Ga<sub>x</sub>Fe<sub>2-x</sub>O<sub>3</sub> epitaxial thin films, *Adv. Funct. Mater.*, 2018, **28**, 1704789.
- 22 T. Katayama, S. Yasui, T. Osakabe, Y. Hamasaki and M. Itoh, Ferrimagnetism and ferroelectricity in Cr-substituted GaFeO<sub>3</sub> epitaxial films, *Chem. Mater.*, 2018, **30**, 1436.
- 23 T. Katayama, S. Yasui, Y. Hamasaki, T. Osakabe and M. Itoh, Chemical tuning of room-temperature ferrimagnetism and ferroelectricity in  $\epsilon$ -Fe<sub>2</sub>O<sub>3</sub>-type multiferroic oxide thin films, *J. Mater. Chem. C*, 2017, **5**, 12597.
- 24 M. Trassin, N. Viart, G. Versini, J.-L. Loison, J.-P. Vola, G. Schmerber, O. Crégut, S. Barre, G. Pourroy, J. H. Lee, W. Jo and C. Mény, Epitaxial thin films of multiferroic GaFeO<sub>3</sub> on conducting indium tin oxide (001) buffered yttrium-stabilized zirconia (001) by pulsed laser deposition, *Appl. Phys. Lett.*, 2007, **91**, 202504.
- 25 A. Thomasson, S. Cherifi, C. Lefevre, F. Roulland, B. Gautier, D. Albertini, C. Meny and N. Viart, Room temperature multiferroicity in Ga<sub>0.6</sub>Fe<sub>1.4</sub>O<sub>3</sub>:Mg thin films, *J. Appl. Phys.*, 2013, **113**, 214101.
- 26 T. Rojac, A. Bencan, G. Drazic, N. Sakamoto, H. Ursic, B. Jancar, G. Tavcar, M. Makarovic, J. Walker, B. Malic and D. Damjanovic, Domain-wall conduction in ferroelectric BiFeO<sub>3</sub> controlled by accumulation of charged defects., *Nat. Mater.*, 2017, **16**, 322–327.
- 27 X. Guan, L. Yao, K. Z. Rushchanskii, S. Inkinen, R. Yu, M. Ležaić, F. Sánchez, M. Gich and S. Dijken, Unconventional Ferroelectric Switching via Local Domain Wall Motion in Multiferroic  $\epsilon$ -Fe<sub>2</sub>O<sub>3</sub> Films, *Adv. Electron. Mater.*, 2020, **6**, 1901134.
- 28 D. Stoeffler, First principles study of the electric polarization and of its switching in the multiferroic GaFeO<sub>3</sub> system, *J. Phys.: Condens. Matter*, 2012, **24**, 185502.
- 29 C. A. Randall, N. Kim, J. Kucera, W. Cao and T. R. Shrout, Intrinsic and Extrinsic Size Effects in Fine-Grained Morphotropic-Phase-Boundary Lead Zirconate Titanate Ceramics, *J. Am. Ceram. Soc.*, 1998, **81**, 677.

